A Radio-Frequency Ion Trap System for the Multi-Reflection Time-of-Flight Mass Spectrometer at SHANS and Its Offline Commissioning

Jun-Ying Wang [1,2], **Wen-Xue Huang** [1,2,3,*], **Yu-Lin Tian** [1,2,3,*], **Yong-Sheng Wang** [1,2,3,4], **Yue Wang** [1,2], **Wan-Li Zhang** [1,3], **Yuan-Jun Huang** [5], **Zai-Guo Gan** [1,2,3] and **Hu-Shan Xu** [1,2,3]

1   Institute of Modern Physics, Chinese Academy of Sciences, Lanzhou 730000, China
2   Advanced Energy Science and Technology Guangdong Laboratory, Huizhou 516000, China
3   School of Nuclear Science and Technology, University of Chinese Academy of Sciences, Beijing 100049, China
4   School of Nuclear Science and Technology, Lanzhou University, Lanzhou 730000, China
5   School of Aeronautics and Astronautics, University of Electronic Science and Technology of China, Chengdu 611731, China
*   Correspondence: huangwx@impcas.ac.cn (W.-X.H.); yltianok@impcas.ac.cn (Y.-L.T.)

Abstract: To precisely measure atomic masses and select neutron-deficient isotopes produced by fusion evaporation reactions, an MRTOF-MS (multi-reflection time-of-flight mass spectrometer) at the SHANS (Spectrometer for Heavy Atom and Nuclear Structure) is being developed. One of the key parts, an RF ion trap system with the aim to provide brilliant ion pulses with a low energy spread and narrow pulse width for ion preparation prior to injection into the MRTOF mass analyzer, has been constructed and commissioned offline successfully. The principle, construction details and test results are reported. Pulsed beams of $^{39}K^{1+}$, $^{85,87}Rb^{1+}$ and $^{133}Cs^{1+}$ ions have been tested and the amplitudes and frequencies of the RF signals, DC voltages, helium gas pressure and time parameters have been scanned. The corresponding time spreads have reached 0.252 µs, 0.394 µs and 0.450 µs, respectively.

Keywords: multi-reflection time-of-flight mass spectrometer; mass measurement; ion trap; radio frequency

1. Introduction

With the advantages of single-ion sensitivity, a non-scanning nature, a large mass range, a short measurement time and less expensive construction cost compared to storage rings and/or Penning traps, multi-reflection time-of-flight (MRTOF) devices [1–14] used in nuclear physics applications have been developing very quickly in recent years. Many gratifying results have been achieved [15–23]. To precisely measure atomic masses and select neutron-deficient isotopes produced by fusion evaporation reactions, a multi-reflection time-of-flight mass spectrometer (MRTOF-MS) at the Spectrometer for Heavy Atom and Nuclear Structure (SHANS) [24] is being developed at the Institute of Modern Physics, Chinese Academy of Sciences (IMP/CAS). The SHANS is a gas-filled recoil separator with a QDQQ magnetic configuration, where D and Q denote the dipole and quadrupole magnets, respectively, and the maximum magnetic rigidity of the dipole magnet is 2.9 Tm. New isotopes in the actinide region, $^{204,205}Ac$, ^{207}Th, $^{214-216}U$ and $^{219,220,222-224}Np$, have been synthesized and their decay properties studied experimentally at the SHANS. The study of heavy and super-heavy nuclei and elements at the IMP/CAS has been reviewed in ref. [25].

Figure 1 shows a sketch of the MRTOF-MS at the SHANS. For the reason of space limitations behind the SHANS, we adopt a concomitant referencing mode [26] instead of the linear configuration we previously described in ref. [27]. The MRTOF-MS can be divided into three parts according to their tasks: the cryogenic gas catcher (CGC), the radio-frequency (RF) ion trap system and the MRTOF mass analyzer. The separated evaporation

residues (ERs) from the SHANS with kinetic energies at a few tens of MeV are decelerated using a degrader, stopped in the CGC filled with helium gas and transported by the electrostatic field of the DC cage (see Figure 1) together with the "ion surfing" method with a radio frequency carpet [28–32]. The ions are extracted out of the gas catcher and transported through a large acceptance quadrupole ion beam guide (QPIG) into the RF ion trap system, where the ions are accumulated, cooled and pulsed. The bunched ions are accelerated to 1500 eV using an acceleration pulsed drift tube (Acc-PDT) and shot into the mass analyzer. After flying hundreds of revolutions in the analyzer, the ions with different mass-to-charge ratios are separated and released, and they hit the detector where the times of flight of the ions are measured, and thus the masses of the ions are analyzed. The Acc-PDT is use to match the energy requirement of the mass analyzer.

The mass analyzer has been constructed and commissioned offline successfully, and the details of the offline commissioning and the achieved performances have been reported in ref. [14]. The mass resolving power has reached 90,000 with a time of flight of $\sim$20 ms with a chopped $^{133}Cs^{1+}$ beam using a Bradbury–Nielsen gate [33] with the optimized opening time of 0.15 µs. For a higher mass resolving power, a pulsed beam with a narrower width is needed at least. Generally speaking, an optimal time-of-flight measurement by the MRTOF mass analyzer needs ions to be injected as brilliant pulses, with a low energy spread, narrow width and well alignment to the optical axis of the analyzer. To achieve these requirements, the RF ion trap system has been constructed. In addition, for collecting recoils separated by the SHANS and transporting them to the RF ion trap system, a CGC, including a DC cage and an RF carpet, is being constructed.

In this paper, we will concentrate on the RF ion trap system and its offline commissioning and report the achieved performances.
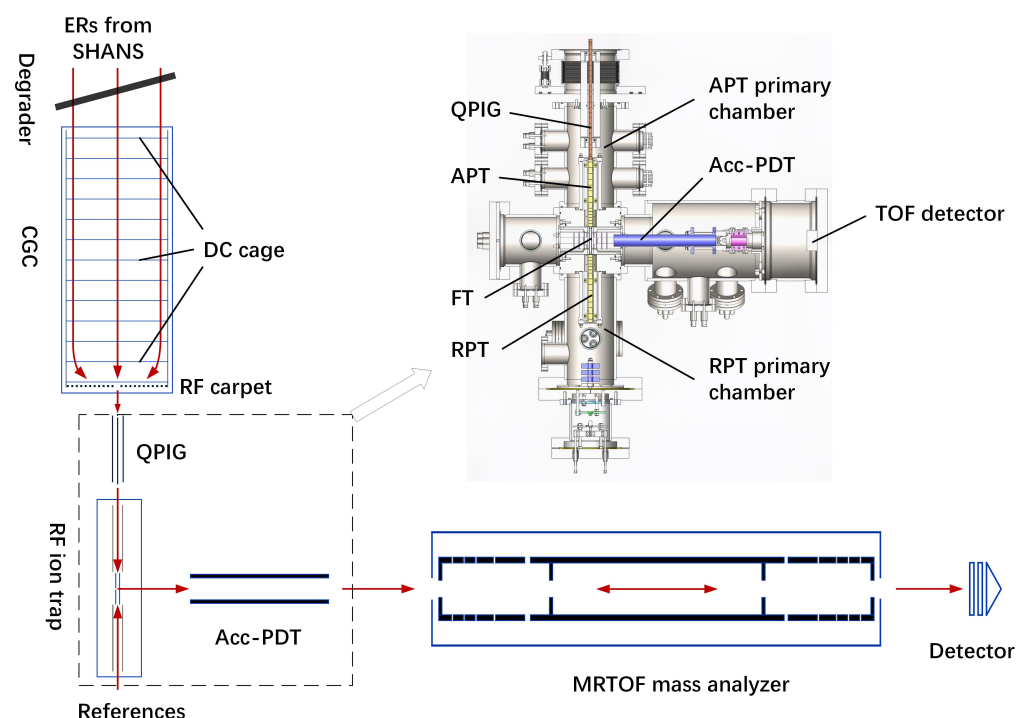

Figure 1. Sketch of the MRTOF-MS at SHANS and the cross-section drawing of mechanic design of the RF ion trap system, in which a TOF detector has been attached temporarily for the experiments reported in this paper. The red arrows show the direction of beam transportation. CGC: cryogenic gas catcher; QPIG: quadrupole ion beam guide; APT: analyte Paul trap; RPT: reference Paul trap; FT: flat trap; Acc-PDT: acceleration pulsed drift tube. See text for details.

2. Experimental Setup

As shown in Figures 1 and 2a, the RF ion trap system consists of an analyte Paul trap (APT), a reference Paul trap (RPT) and a flat trap (FT). The structures of both the APT and RPT are the same, and they are assembled symmetrically. The radio frequency quadrupole (RFQ) technique is used to confine ions in the transverse directions, and buffer gas is used to cool ions [34]. Configurable DC potentials on the segmented RFQ are employed to manipulate ions in the longitudinal direction. The analytes and references are accumulated and pre-cooled in the APT and RPT, respectively, and they are ejected orthogonally from the FT after further cooling.

The ion motion in the RF ion trap system in one measurement cycle is illustrated in Figure 2b–e. The references are transferred to the FT by lowering the potentials of the RPT's last segments and FT's axial outermost electrode, while the analytes are being accumulated in the APT. The references are cooled down and extracted out orthogonally from the FT through a hole in the center of its board by changing the potentials of two central plate electrodes after a certain cooling time, then the pulsed reference bunch will be sent to the MRTOF mass analyzer for TOF measurement. During this period, analytes and subsequent references are accumulated in their Paul traps simultaneously. Afterwards, the analytes accumulated in the APT are transferred, cooled, extracted and measured in the same way. In this RF ion trap system, ions can be cooled rapidly and effectively so that short-lived isotopes with a half-life of a few milliseconds can be measured.
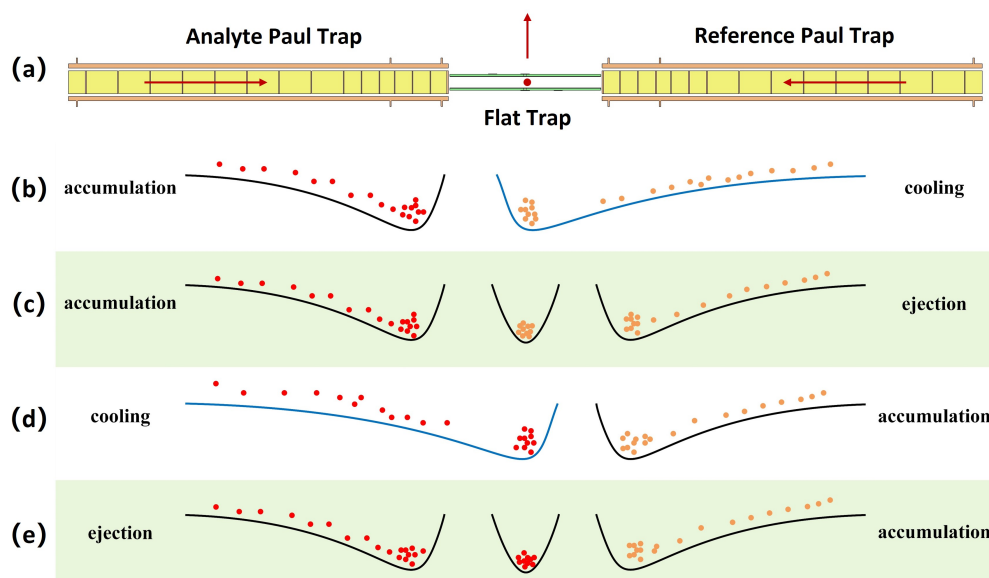

Figure 2. (**a**) Sketch of the RF ion trap system. The red arrows show the direction of beam transportation. (**b**–**e**) Diagram of ion motion in the RF ion trap system. See text for details.

The traps are realized using the printed circuit board (PCB) technique [26]. The APT/RPT is formed using four PCB strips, and each strip has a length of 133.7 mm and a width of 8 mm with 15 segments, as shown in Figure 3b. Electrodes are connected by thin film surface-mounted resistors of 100 kΩ and capacitors of 1 nF on the back side. The adjacent strips are supplied with RF voltages of an equal amplitude but opposite phases. The DC voltages are applied at the two outermost electrodes (DC1 and DC3 in Figure 3) as well as the twelfth one (DC2) along the direction of beam transportation. The three DC voltages can be switched rapidly and simultaneously to generate either a DC potential well to axially confine ions or an axial gradient to transfer ions to the FT. The typical DC potentials are listed in Figure 3a and the corresponding axial potential distribution calculated with SIMION [35] is shown in Figure 3c.
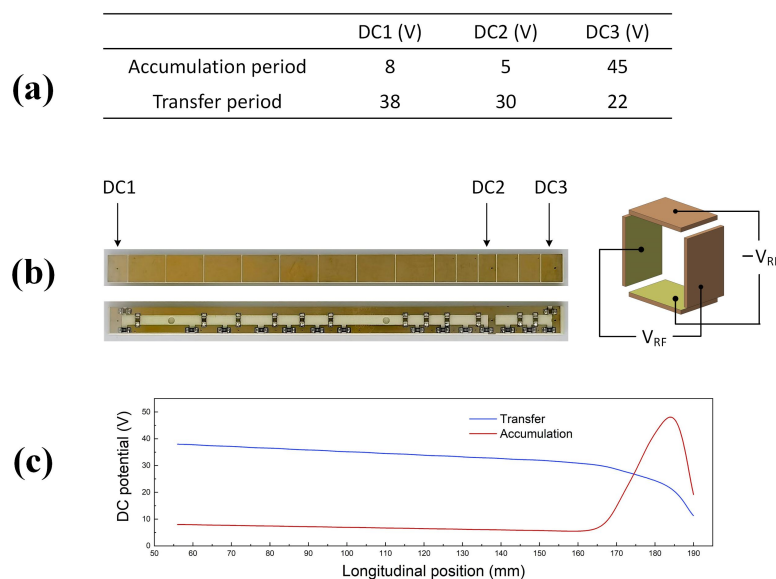
	DC1 (V)	DC2 (V)	DC3 (V)
Accumulation period	8	5	45
Transfer period	38	30	22

(a)

(b)

(c)

Figure 3. (**a**) Typical DC potentials of the accumulation and transfer period applied on the APT/RPT. (**b**) Photographs of the front and back sides of one segmented strip of APT/RPT and the cross-section of APT/RPT. (**c**) DC potential of the APT/RPT along the axis calculated with SIMION [35].

The FT uses a "flat" geometry, which is conducive to form a well-defined dipole field at the trap center to extract ions. The basic components of the FT are two PCBs mounted in a square chamber, and there is a 4 mm face-to-face spacing between them. Each PCB consists of three strips, as shown in Figure 4b. The middle one has a dimension of 52.7 mm by 5 mm and is divided into 7 segments. Both electrodes labeled with DC4 in the middle of the strip have a hole with a diameter of 0.8 mm at its center. DC potentials are applied on the middle strips to generate a well along the axis, while an RF signal is applied to the four outer strips to provide a radial confining pseudo-potential.
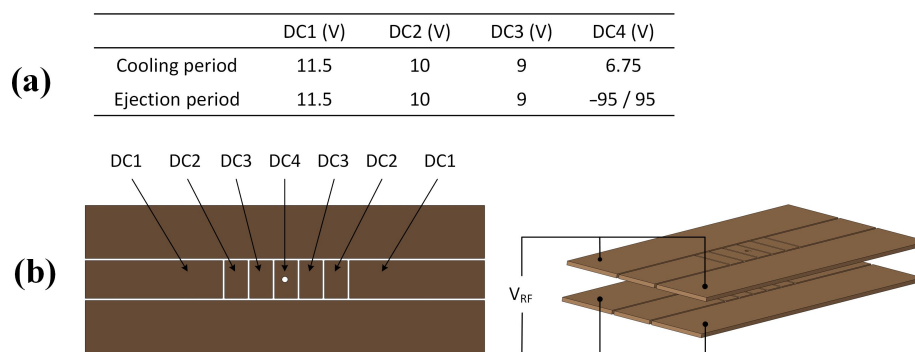
	DC1 (V)	DC2 (V)	DC3 (V)	DC4 (V)
Cooling period	11.5	10	9	6.75
Ejection period	11.5	10	9	–95 / 95

(a)

(b)

Figure 4. (**a**) Typical DC potentials of the FT. (**b**) Illustration of one PCB of FT and the whole FT.

The buffer gas distribution and the corresponding vacuum system are very important and subtle to the RF ion trap system. The helium buffer gas pressure in the APT, RPT and FT should be at the level of $\sim 10^{-3}$–10^{-2} mbar for effective cooling to trap and store ions, while the residual gas pressure in the MRTOF mass analyzer must be better than 1×10^{-7} mbar for a high mass resolving power. Thus, the buffer gas volume must be well sealed and differential pumping must be carefully taken into consideration.

Helium buffer gas is fed into the system by two feeding lines connected to the CGC and the FT region, and it diffuses into the chambers housing the APT, RPT and FT. These three chambers are mounted at the place between the so-called APT and RPT primary vacuum chambers (see Figures 1 and 5). In order to ensure a stable gas pressure and flow, only two holes with a diameter of 0.8 mm in the center of the FT mentioned above and another two ports at the entrance end of the APT and RPT with dimensions of 10 mm by 10 mm

are remained for ion transportation. The primary vacuum chambers and the Acc-PDT region are pumped by turbo molecular pumps (TMPs). Due to the limited space to monitor the pressure directly, the pressure in each trap can only be estimated from indications of the vacuum gauges mounted on the primary vacuum chambers as well as the gas feeding system.

To prove whether this configuration can meet the requirements of vacuum and pressure in each chamber, we simulated it with Molflow [36]. Figure 5 shows the equivalent model. Each chamber is denoted by a cylinder and gas can only flow to other chambers through small holes. The APT, RPT and FT chambers are regarded as one chamber because we thought their pressures should be in the same order of magnitude due to their structures. The pressure in the CGC was set to 100 mbar at room temperature. Under this configuration and the speeds of TMPs shown in Figure 5, the pressures in the APT primary chamber and in the APT/RPT/FT chambers are 7×10^{-2} mbar, and that in the RPT primary chamber is 7×10^{-3} mbar. The vacuum in the Acc-PDT region after the FT is better than 1×10^{-5} mbar.

Based on the results of the simulation, two HiPace 700 TMPs from Pfeiffer Vacuum [37] were employed for the APT primary chamber and the Acc-PDT region, and a TURBOVAC 90 i TMP from Leybold [38] was used for the RPT primary chamber. The pressures in these regions were measured using PTR 90 N PENNINGVAC vacuum gauges from Leybold [38]. The background pressures in the APT and RPT primary chambers were measured to be 2.0×10^{-7} and 5.9×10^{-6} mbar, respectively, while that in the Acc-PDT region was 2.4×10^{-7} mbar. The speed of the TMP at the APT primary chamber was changed between 20 and 100% of its maximum to keep an optimal gas pressure in the regions of the APT and FT. When filling helium gas into the CGC with a pressure of 1.44 mbar and into the FT with 0.11 mbar measured by a gauge at the outlet of the gas feeding line, pressures of 2.6×10^{-3} and 8.7×10^{-4} mbar were obtained at the APT and RPT primary chambers, respectively. Similarly, with a pressure of 13.0 mbar into the CGC and the same 0.11 mbar into the FT, pressures of 2.9×10^{-3} and 9.1×10^{-4} mbar were obtained after increasing the speed of the TMP at the APT primary chamber. The pressure in the Acc-PDT region was better than 9×10^{-7} mbar with gas filling. A much higher gas pressure in the CGC has not yet been tested.
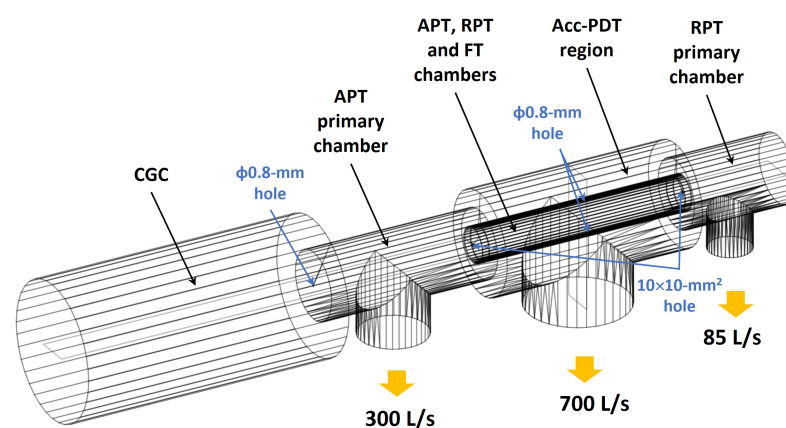

Figure 5. Model in Molflow [36] and typical speeds of TMPs. See text for details.

3. Offline Commissioning

The RF ion trap system has been tested independently without the CGC or the MRTOF mass analyzer. As shown in Figure 6, a continuous $^{133}Cs^{1+}$, $^{85,87}Rb^{1+}$ or $^{39}K^{1+}$ beam is produced by a heated alkali ion source emitter from HeatWave Labs [39] followed by a skimmer, an extraction electrode and an einzel lens. The emitter is connected to a supporting electrode floating at a potential of 28 V above the ground, thereby defining the initial kinetic energy of the ions. The ions are accumulated and pre-cooled in the RPT and cooled further in the FT and pulsed by changing the potentials of two central plate

electrodes of the FT. The typical frequency and amplitude of the RF signal for $^{133}Cs^{1+}$ at the RPT are 2.350 MHz and 300 V_{pp}, respectively, and those at the FT are 2.130 MHz and 850 V_{pp}. The RF signals are fed to the electrodes using homemade matching circuits. After extraction from the FT, ions are accelerated by three plate electrodes, pass through the Acc-PDT and the deflector, and impact on the detector at last, which is a MagneTOF mini from ETP [40]. Ion bunches should be accelerated in the Acc-PDT to appropriate kinetic energy to match the requirement of the MRTOF mass analyzer, and the misalignment of the axes between the FT and mass analyzer could be corrected by applying different voltages on the deflector. But during the offline test we only applied -400 V on the Acc-PDT and -600 V on the deflector because neither energy matching nor misalignment correction is needed during this period. A blind flange is used to seal the chamber on the APT side. The electrodes of the APT are set on high potentials, the same as that in the accumulation period of analytes shown in Figure 3a. The typical operating parameters are shown in Figure 6.
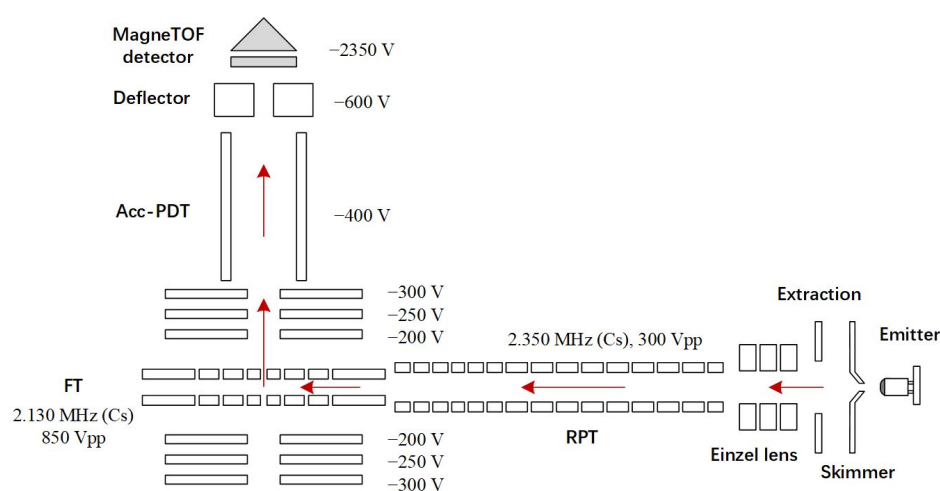

Figure 6. Sketch of offline commissioning of the RF ion trap system without the CGC or the MRTOF mass analyzer. The red arrows show the direction of beam transportation.

The switches used for the DC voltage switching of the APT and RPT are AMX1500 modules from CGC Instruments [41], and those for the FT are GHTS 60 products from BEHLKE Power Electronics [42]. The TOF starts when the ions are extracted from the FT and stops when they impact on the detector, where the signal is acquired by a multiple-event time digitizer MCS8A from FAST ComTec [43]. The whole system is controlled remotely by a specialized distributed real-time control system based on EPICS [44], which is extended from the control system described in ref. [14].

Pulsed beams of $^{39}K^{1+}$, $^{85,87}Rb^{1+}$ and $^{133}Cs^{1+}$ ions have been tested, and the amplitudes and frequencies of the RF signals, DC voltages, helium gas pressure and time parameters have been scanned carefully. In our test, a typical accumulation time in the RPT of 2–3 ms and a cooling time in the FT of 2–4 ms according to various gas pressures and ion masses are obtained. Figure 7 shows counts per pulse and time spread of the TOF depending on the cooling time of $^{133}Cs^{1+}$ in the FT under different gas pressures measured by a gauge at the outlet of the gas feeding line near the FT. As the cooling time increases, the counts per pulse of the ions increase and reach a plateau after 1 ms, while the time spread of the TOF decreases and reaches the minimum at the same time. According to the results, most ions can be cooled in 2 ms. As the gas pressure increases from 0.130 to 0.148 mbar, the counts per pulse of the ions increase, reach the maximum at 0.146 mbar and decrease. This behavior can be explained by the effective cooling of the ions in the FT. With effective cooling, the ions will stay at the bottom of the pseudo-potential well produced by RF signals and the well produced by axial DC potentials, and the beam size will be smaller, and thus the ions can go through the 0.8 mm diameter hole and be extracted more effectively out from the FT. With a lower pressure than the optimal value, the ions cannot

be cooled enough. This can be improved by increasing the cooling time, which is confirmed by Figure 7. With a higher pressure than the optimal one, the ions may be heated by the collisions with the buffer gas, and the beam size becomes larger. It means that the buffer gas pressure must be optimized for effective cooling to obtain a high efficiency. Figure 8 shows the TOF spectra of $^{39}K^{1+}$, $^{85,87}Rb^{1+}$ and $^{133}Cs^{1+}$. The time spread for these masses have been reached at 0.252 μs, 0.394 μs and 0.450 μs, respectively.

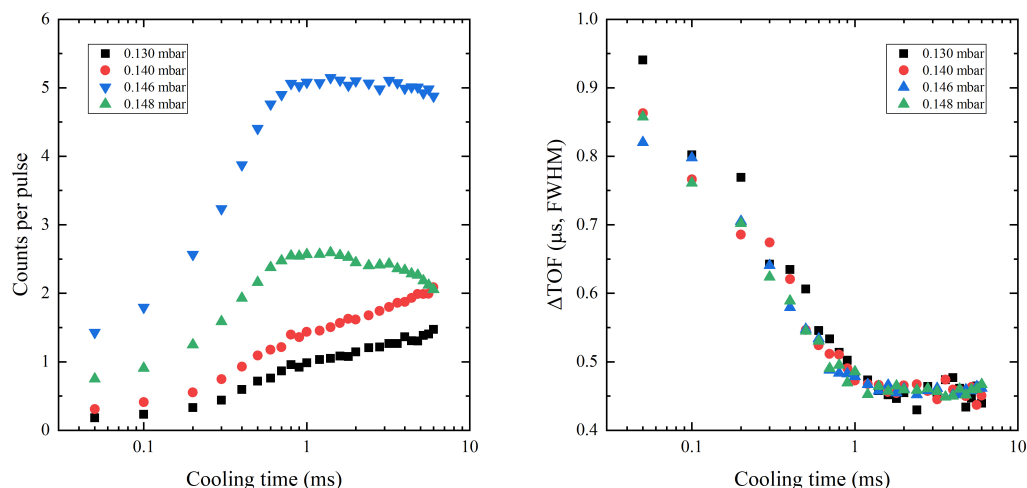**Figure 7.** Counts per pulse (**left**) and time spread of TOF (**right**) depending on the cooling time of $^{133}Cs^{1+}$ in the FT under different gas pressures measured by a gauge at the outlet of the gas feeding line near the FT.
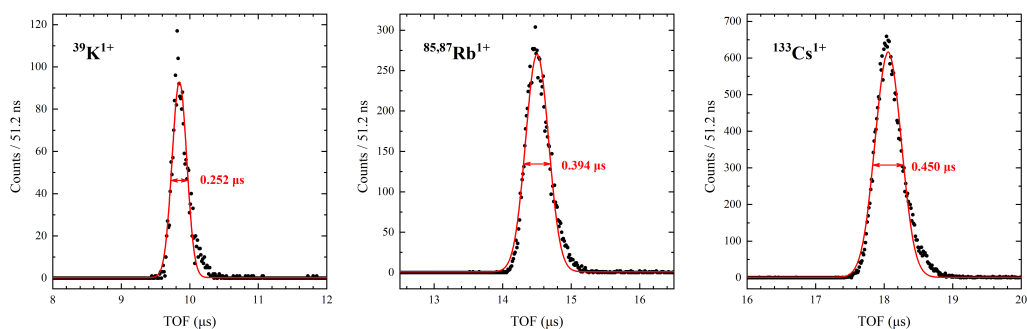

Figure 8. TOF spectra of $^{39}K^{1+}$, $^{85,87}Rb^{1+}$ and $^{133}Cs^{1+}$ and the corresponding time spread of TOF. The red curves are the fitted results with a Gaussian function.

The results show that this RF ion trap system successfully realizes the accumulation of ions in the RPT, the storage and cooling in the FT, and the extraction of ions out from the FT to form a pulsed beam, which satisfies the requirement of the MRTOF mass analyzer downstream. Due to the same structure of the APT and RPT, it is foreseen that the ions from the CGC can also be smoothly transported, accumulated, cooled and pulsed. The $^{39}K^{1+}$, $^{85,87}Rb^{1+}$ and $^{133}Cs^{1+}$ ions, which have a relative mass precision of better than 1.5×10^{-10}, will be the references in the studies of heavy and super-heavy nuclei to calibrate the TOF drift caused by the inaccuracy of potentials applied on the electrodes, the long time drift of electronics, the variation in temperature and electric power, etc. In order to obtain a better pulsed beam with a narrower time distribution, fast switches and a matching circuit will be optimized further in the near future.

4. Summary

An RF ion trap system for the MRTOF-MS at the SHANS has been constructed and commissioned offline successfully. Specialized systems for the vacuum, power supply, control and data acquisition have been developed. The $^{39}K^{1+}$, $^{85,87}Rb^{1+}$ and $^{133}Cs^{1+}$ ions

have been measured in the offline test, and the corresponding time spreads of the TOF have been measured to be 0.252 µs, 0.394 µs and 0.450 µs, respectively.

References

1. Wolf, R.N.; Beck, D.; Blaum, K.; Bohm, C.; Borgmann, C.; Breitenfeldt, M.; Herfurth, F.; Herlert, A.; Kowalska, M.; Kreim, S.; et al. On-line separation of short-lived nuclei by a multi-reflection time-of-flight device. *Nucl. Instrum. Methods A* **2012**, *686*, 82–90. [CrossRef]
2. Dickel, T.; Plaß, W.R.; Becker, A.; Czok, U.; Geissel, H.; Haettner, E.; Jesch, C.; Kinsel, W.; Petrick, M.; Scheidenberger, C.; et al. A high-performance multiple-reflection time-of-flight mass spectrometer and isobar separator for the research with exotic nuclei. *Nucl. Instrum. Methods A* **2015**, *777*, 172–188. [CrossRef]
3. Schury, P.; Wada, M.; Ito, Y.; Arai, F.; Naimi, S.; Sonoda, T.; Wollnik, H.; Shchepunov, V.A.; Smorra, C.; Yuan, C. A high-resolution multi-reflection time-of-flight mass spectrograph for precision mass measurements at RIKEN/SLOWRI. *Nucl. Instrum. Methods B* **2014**, *335*, 39–53. [CrossRef]
4. Schury, P.; Wada, M.; Ito, Y.; Kaji, D.; Arai, F.; MacCormick, M.; Murray, I.; Haba, H.; Jeong, S.; Kimura, S.; et al. First online multireflection time-of-flight mass measurements of isobar chains produced by fusion-evaporation reactions: Toward identification of superheavy elements via mass spectroscopy. *Phys. Rev. C* **2017**, *95*, 011305. [CrossRef]
5. Hirsh, T.Y.; Paul, N.; Burkey, M.; Aprahamian, A.; Buchinger, F.; Caldwell, S.; Clark, J.A.; Levand, A.F.; Ying, L.L.; Marley, S.T.; et al. First operation and mass separation with the CARIBU MR-TOF. *Nucl. Instrum. Methods B* **2016**, *376*, 229–232. [CrossRef]
6. Kolhinen, V.S.; Eronen, T.; Gorelov, D.; Hakala, J.; Jokinen, A.; Jokiranta, K.; Kankainen, A.; Koikkalainen, M.; Koponen, J.; Kulmala, H.; et al. Recommissioning of JYFLTRAP at the new IGISOL-4 facility. *Nucl. Instrum. Methods B* **2013**, *317*, 506–509. [CrossRef]
7. Chauveau, P.; Delahaye, P.; De France, G.; El Abir, S.; Lory, J.; Merrer, Y.; Rosenbusch, M.; Schweikhard, L.; Wolf, R.N. PILGRIM, a Multi-Reflection Time-of-Flight Mass Spectrometer for SPIRAL2-S^3 at GANIL. *Nucl. Instrum. Methods B* **2016**, *376*, 211–215. [CrossRef]
8. Tian, Y.L.; Wang, Y.S.; Wang, J.Y.; Zhou, X.H.; Huang, W.X. Designing a multi-reflection time-of-flight mass analyzer for LPT. *Int. J. Mass Spectrom.* **2016**, *408*, 28–32. [CrossRef]
9. Huang, W.X.; Tian, Y.L.; Wang, Y.S.; Wang, J.Y.; Zhou, X.H. Optimization of multi-reflection time-of-flight mass analyzer operating in in-trap-lift mode. *Radiat. Detect. Technol. Methods* **2018**, *2*, 1. [CrossRef]
10. Yoon, J.W.; Park, Y.H.; Im, K.B.; Kim, G.D.; Kim, Y.K. Design study for a multi-reflection time-of-flight mass spectrograph for very short lived nuclei. In Proceedings of the Conference on Advances in Radioactive Isotope Science (ARIS2014), Tokyo, Japan, 1–6 June 2014. [CrossRef]
11. Liu, B.; Brodeur, M.; Burdette, D.P.; Kelly, J.M.; Kim, T.; Long, J.; O'Malley, P.D. The performance of the commissioned Notre Dame multi-reflection time-of-flight mass spectrometer. *Nucl. Instrum. Methods A* **2021**, *985*, 164679. [CrossRef]
12. Reiter, M.; Andrés, S.A.S.; Bergmann, J.; Dickel, T.; Dilling, J.; Jacobs, A.; Kwiatkowski, A.; Plaß, W.; Scheidenberger, C.; Short, D.; et al. Commissioning and performance of TITAN's Multiple-Reflection Time-of-Flight Mass-Spectrometer and isobar separator. *Nucl. Instrum. Methods A* **2021**, *1018*, 165823. [CrossRef]
13. Yavor, M.I.; Gall, N.R.; Muradymov, M.Z.; Pomozov, T.V.; Kurnin, I.V.; Monakov, A.G.; Arsenev, A.N.; Oganessian, Y.T.; Karpov, A.V.; Rodin, A.M.; et al. Development of a mass spectrometer for high-precision mass measurements of superheavy elements at JINR. *J. Instrum.* **2022**, *17*, P11033. [CrossRef]
14. Huang, W.X.; Wang, Y.S.; Tian, Y.L.; Wang, J.Y.; Wang, Y.; Gan, Z.G.; Xu, H.S. Offline commissioning and performance of a multi-reflection time-of-flight mass analyzer with a new configuration. *Nucl. Instr. Methods A* **2023**, *1047*, 167825. [CrossRef]

15. Wienholtz, F.; Beck, D.; Blaum, K.; Borgmann, C.; Breitenfeldt, M.; Cakirli, R.B.; George, S.; Herfurth, F.; Holt, J.D.; Kowalska, M.; et al. Masses of exotic calcium isotopes pin down nuclear forces. *Nature* **2013**, *498*, 346–349. [CrossRef] [PubMed]

16. Atanasov, D.; Ascher, P.; Blaum, K.; Cakirli, R.B.; Cocolios, T.E.; George, S.; Goriely, S.; Herfurth, F.; Janka, H.T.; Just, O.; et al. Precision Mass Measurements of $^{129-131}$Cd and Their Impact on Stellar Nucleosynthesis via the Rapid Neutron Capture Process. *Phys. Rev. Lett.* **2015**, *115*, 232501. [CrossRef]

17. Rosenbusch, M.; Ascher, P.; Atanasov, D.; Barbieri, C.; Beck, D.; Blaum, K.; Borgmann, C.; Breitenfeldt, M.; Cakirli, R.B.; Cipollone, A.; et al. Probing the $N = 32$ Shell Closure below the Magic Proton Number $Z = 20$: Mass Measurements of the Exotic Isotopes ^{52,53}K. *Phys. Rev. Lett.* **2015**, *114*, 202501. [CrossRef]

18. Leistenschneider, E.; Reiter, M.P.; Ayet San Andrés, S.; Kootte, B.; Holt, J.D.; Navrátil, P.; Babcock, C.; Barbieri, C.; Barquest, B.R.; Bergmann, J.; et al. Dawning of the $N = 32$ Shell Closure Seen through Precision Mass Measurements of Neutron-Rich Titanium Isotopes. *Phys. Rev. Lett.* **2018**, *120*, 062503. [CrossRef]

19. Ito, Y.; Schury, P.; Wada, M.; Arai, F.; Haba, H.; Hirayama, Y.; Ishizawa, S.; Kaji, D.; Kimura, S.; Koura, H.; et al. First Direct Mass Measurements of Nuclides around $Z = 100$ with a Multireflection Time-of-Flight Mass Spectrograph. *Phys. Rev. Lett.* **2018**, *120*, 152501. [CrossRef] [PubMed]

20. Schury, P.; Niwase, T.; Wada, M.; Brionnet, P.; Chen, S.; Hashimoto, T.; Haba, H.; Hirayama, Y.; Hou, D.S.; Iimura, S.; et al. First high-precision direct determination of the atomic mass of a superheavy nuclide. *Phys. Rev. C* **2021**, *104*, L021304. [CrossRef]

21. Wolf, R.N.; Beck, D.; Blaum, K.; Bohm, C.; Borgmann, C.; Breitenfeldt, M.; Chamel, N.; Goriely, S.; Herfurth, F.; Kowalska, M.; et al. Plumbing Neutron Stars to New Depths with the Binding Energy of the Exotic Nuclide ^{82}Zn. *Phys. Rev. Lett.* **2013**, *110*, 041101. [CrossRef]

22. Welker, A.; Althubiti, N.A.S.; Atanasov, D.; Blaum, K.; Cocolios, T.E.; Herfurth, F.; Kreim, S.; Lunney, D.; Manea, V.; Mougeot, M.; et al. Binding Energy of ^{79}Cu: Probing the Structure of the Doubly Magic ^{78}Ni from Only One Proton Away. *Phys. Rev. Lett.* **2017**, *119*, 192502. [CrossRef] [PubMed]

23. Niwase, T.; Watanabe, Y.X.; Hirayama, Y.; Mukai, M.; Schury, P.; Andreyev, A.N.; Hashimoto, T.; Iimura, S.; Ishiyama, H.; Ito, Y.; et al. Discovery of New Isotope ^{241}U and Systematic High-Precision Atomic Mass Measurements of Neutron-Rich Pa-Pu Nuclei Produced via Multinucleon Transfer Reactions. *Phys. Rev. Lett.* **2023**, *130*, 132502. [CrossRef]

24. Zhang, Z.Y.; Ma, L.; Gan, Z.G.; Huang, M.H.; Huang, T.H.; Li, G.S.; Wu, X.L.; Jia, G.B.; Yu, L.; Yang, H.B.; et al. A gas-filled recoil separator, SHANS. *Nucl. Instrum. Methods B* **2013**, *317*, 315–318. [CrossRef]

25. Gan, Z.G.; Huang, W.X.; Zhang, Z.Y.; Zhou, X.H.; Xu, H.S. Results and perspectives for study of heavy and super-heavy nuclei and elements at IMP/CAS. *Eur. Phys. J. A* **2022**, *58*, 158. [CrossRef]

26. Schury, P.; Ito, Y.; Rosenbusch, M.; Miyatake, H.; Wada, M.; Wollnik, H. Improving wide-band mass measurements in a multi-reflection time-of-flight mass spectrograph by usage of a concomitant measurement scheme. *Int. J. Mass Spectrom.* **2018**, *433*, 40–46. [CrossRef]

27. Wang, J.Y.; Tian, Y.L.; Wang, Y.S.; Gan, Z.G.; Zhou, X.H.; Xu, H.S.; Huang, W.X. A multi-reflection time-of-flight mass analyzer at IMP/CAS. *Nucl. Instr. Methods B* **2020**, *463*, 179–183. [CrossRef]

28. Wada, M.; Ishida, Y.; Nakamura, T.; Yamazaki, Y.; Kambara, T.; Ohyama, H.; Kanai, Y.; Kojima, T.M.; Nakai, Y.; Ohshima, N.; et al. Slow RI-beams from projectile fragment separators. *Nucl. Instr. Methods B* **2003**, *204*, 570–581. [CrossRef]

29. Bollen, G. "Ion surfing" with radiofrequency carpets. *Int. J. Mass Spectrom.* **2011**, *299*, 131–138. [CrossRef]

30. Schwarz, S. RF ion carpets: The electric field, the effective potential, operational parameters and an analysis of stability. *Int. J. Mass Spectrom.* **2011**, *299*, 71–77. [CrossRef]

31. Hamaker, A.; Brodeur, M.; Kelly, J.M.; Long, J.; Nicoloff, C.; Ryan, S.; Schultz, B.E.; Schury, P.; Wada, M. Experimental investigation of the repelling force from RF carpets. *Int. J. Mass Spectrom.* **2016**, *404*, 14–19. [CrossRef]

32. Jones, B.J.P.; Raymond, A.; Woodruff, K.; Byrnes, N.; Denisenko, A.A.; Foss, F.W.; Navarro, K.; Nygren, D.R.; Vuong, T.T.; Adams, C.; et al. The dynamics of ions on phased radio-frequency carpets in high pressure gases and application for barium tagging in xenon gas time projection chambers. *Nucl. Instrum. Methods A* **2022**, *1039*, 167000. [CrossRef]

33. Bradbury, N.; Nielsen, R. Absolute Values of the Electron Mobility in Hydrogen. *Phys. Rev.* **1936**, *49*, 388–393. [CrossRef]

34. Herfurth, F.; Dilling, J.; Kellerbauer, A.; Bollen, G.; Henry, S.; Kluge, H.J.; Lamour, E.; Lunney, D.; Moore, R.B.; Scheidenberger, C.; et al. A linear radiofrequency ion trap for accumulation, bunching, and emittance improvement of radioactive ion beams. *Nucl. Instr. Methods A* **2001**, *469*, 254–275. [CrossRef]

35. Manura, D.J.; Dahl, D.A. *SIMION 8.0/8.1 User Manual*; Scientific Instrument Services, Inc., Idaho National Laboratory: Idaho Falls, ID, USA, 2011.

36. Available online: https://molflow.web.cern.ch (accessed on 20 August 2023).

37. Available online: http://www.pfeiffer-vacuum.com (accessed on 20 August 2023).

38. Available online: https://www.leybold.com (accessed on 20 August 2023).

39. Available online: https://www.cathode.com/i_alkali.htm (accessed on 20 August 2023).

40. Available online: https://www.etp-ms.com (accessed on 20 August 2023).

41. Available online: http://www.cgc-instruments.com (accessed on 20 August 2023).

42. Available online: https://www.behlke.com (accessed on 20 August 2023).

43.   Available online: https://www.fastcomtec.com (accessed on 20 August 2023).
44.   Available online: https://epics.anl.gov (accessed on 20 August 2023).